Supporting information

A bifunctional heterostructure promoting the kinetics and stability of sulfur cathode in advanced aluminum-sulfur batteries

Xiao Zheng[1#], Xiaoqi Han[1#], Wenjiao Yao[1,2], Liangming Wei[3*], Jie Zhu, [1] Yongbing Tang[1*]

1 Advanced Energy Storage Technology Research Center, Shenzhen Institute of Advanced Technology, Chinese Academy of Sciences, Shenzhen 518055, China

2 Shenzhen Key Laboratory of Energy Materials for Carbon Neutrality, Shenzhen 518055, China

3 Key Laboratory for Thin Film and Microfabrication of the Ministry of Education, Department of Microelectronics and Nanoscience, School of Electronic Information and Electrical Engineering, Shanghai Jiao Tong University, 800, Dongchuan Road, Shanghai, 200240, China

# These authors contribute equally to this work.

*Correspondence: wj.yao@siat.ac.cn (W. Yao); xq.han@siat.ac.cn (X. Han); lmwei@sjtu.edu.cn (L. Wei); tangyb@siat.ac.cn (Y. Tang)

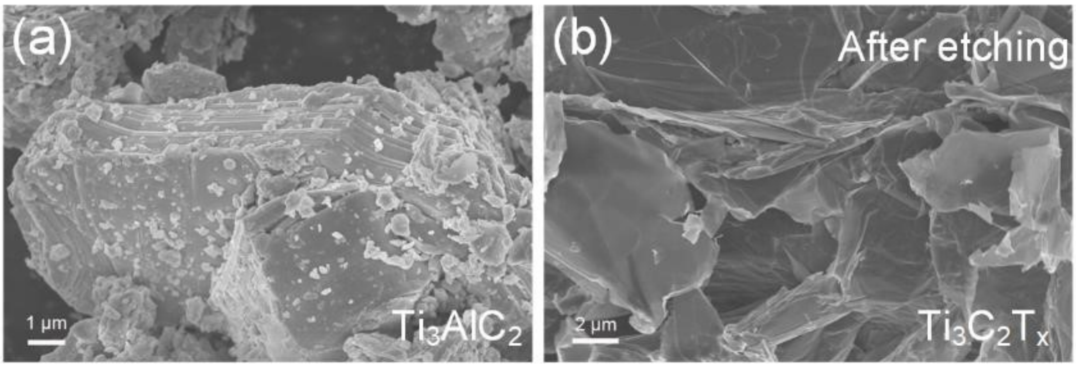

Figure S1. SEM images of (a) Ti_3AlC_2 MAX and (b) multi-layered $Ti_3C_2T_x$.

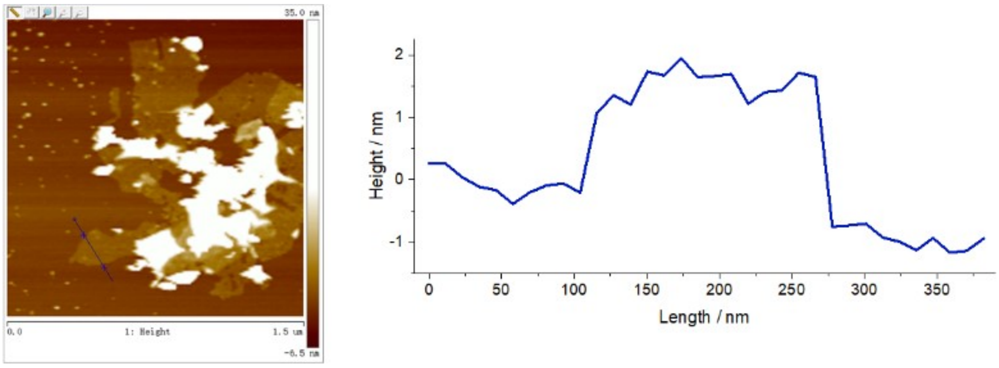

Figure S2. AFM image and the height profile of a $Ti_3C_2T_x$ flake.

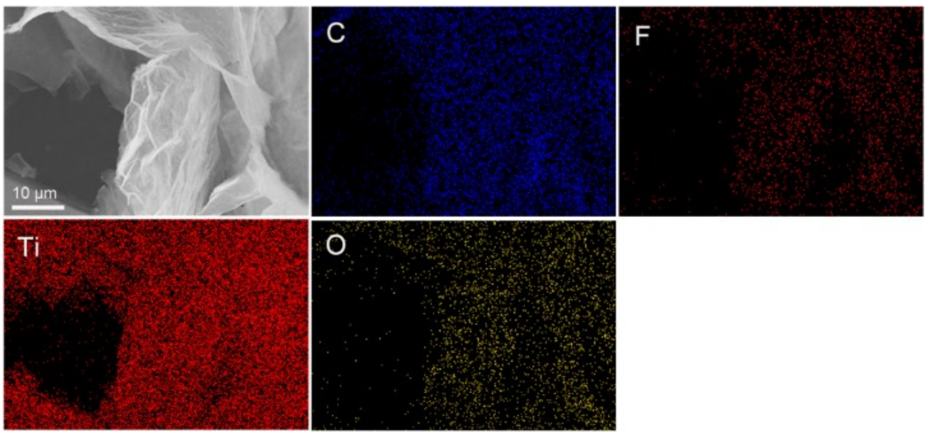

Figure S3. SEM and EDS images of the delaminated $Ti_3C_2T_x$.

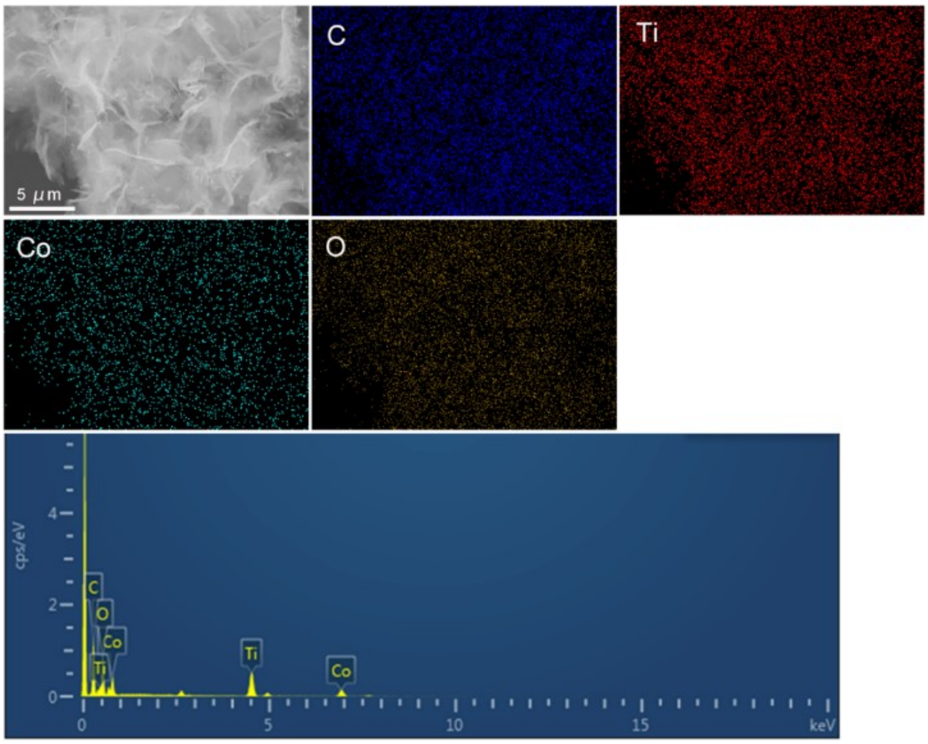

Figure S4. SEM and EDS images of the $Ti_3C_2T_x$-Co composite.

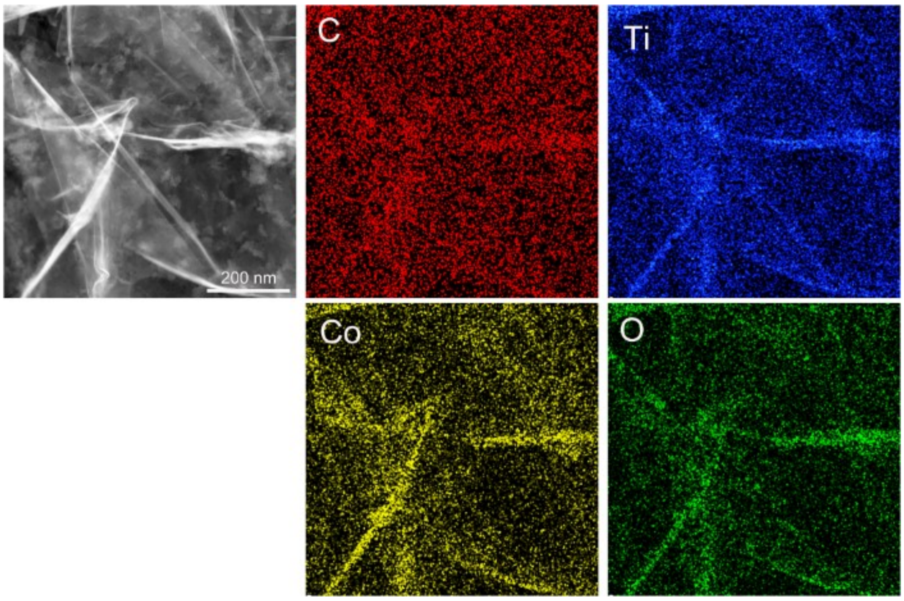

Figure S5. STEM image of the $Ti_3C_2T_x$-Co composite and corresponding EDX elemental mapping images of C, Ti, Co and O.

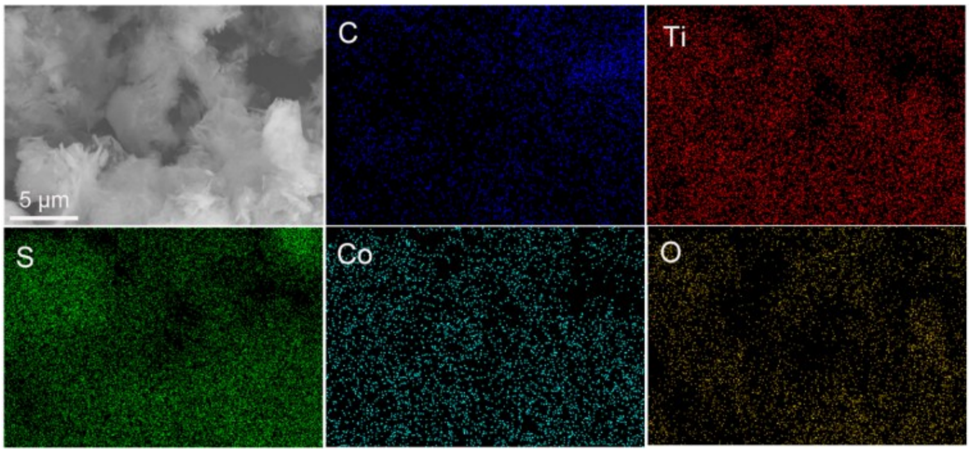

Figure S6. The SEM and EDS images of $Ti_3C_2T_x$-CoS_x@S composite.

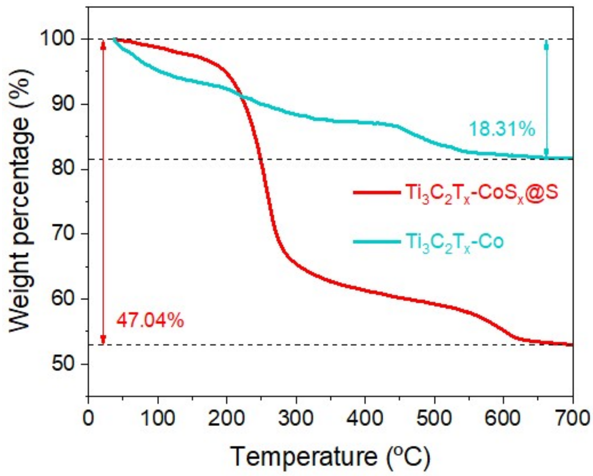

Figure S7. TGA profiles of the $Ti_3C_2T_x$-Co and $Ti_3C_2T_x$-CoS_x@S composite in N_2 atmosphere.

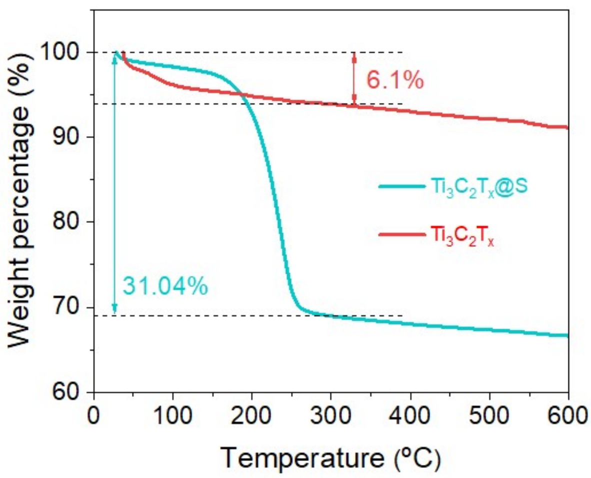

Figure S8. TGA profiles of the $Ti_3C_2T_x$ and $Ti_3C_2T_x$@S composite in N_2 atmosphere.

According to our previous research,[1] the $Ti_3C_2T_x$ host material lost ~6.1% in the same temperature range, presumably due to the release of entrapped structural water. Therefore, the mass fraction of sulfur in the $Ti_3C_2T_x$@S composite is estimated to be ~24.9 wt%.

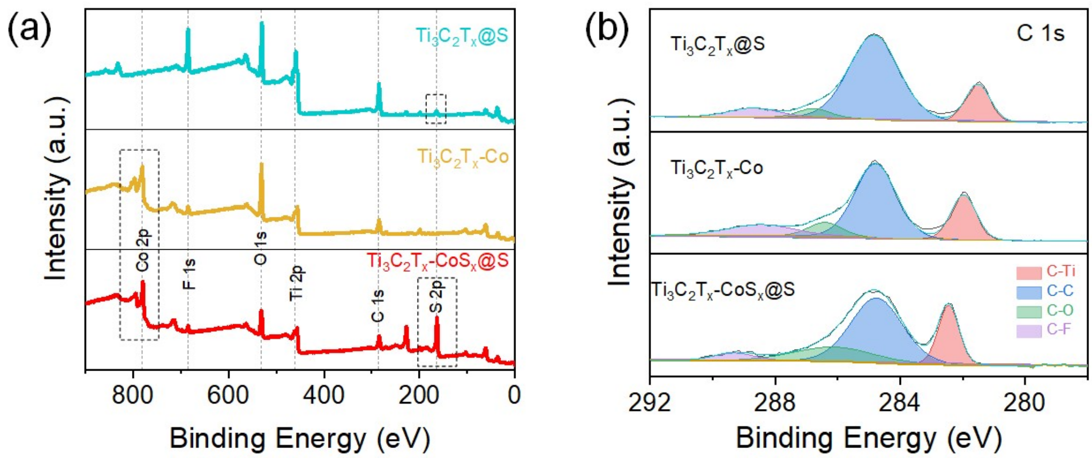

Figure S9. (a) XPS full-spectra of $Ti_3C_2T_x$@S, $Ti_3C_2T_x$-Co and $Ti_3C_2T_x$-CoS_x@S. (b) High-resolution XPS spectra of C 1s in $Ti_3C_2T_x$@S, $Ti_3C_2T_x$-Co and $Ti_3C_2T_x$-CoS_x@S.

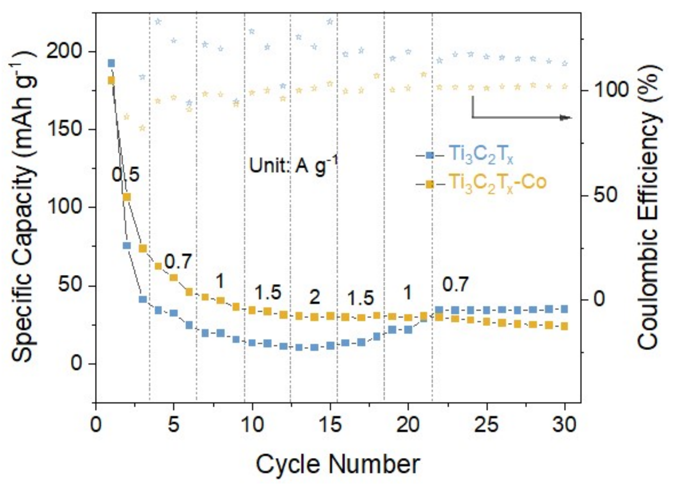

Figure S10. Rate performances of $Ti_3C_2T_x$ and $Ti_3C_2T_x$-Co cathodes from 0.5 to 2 A g^{-1}.

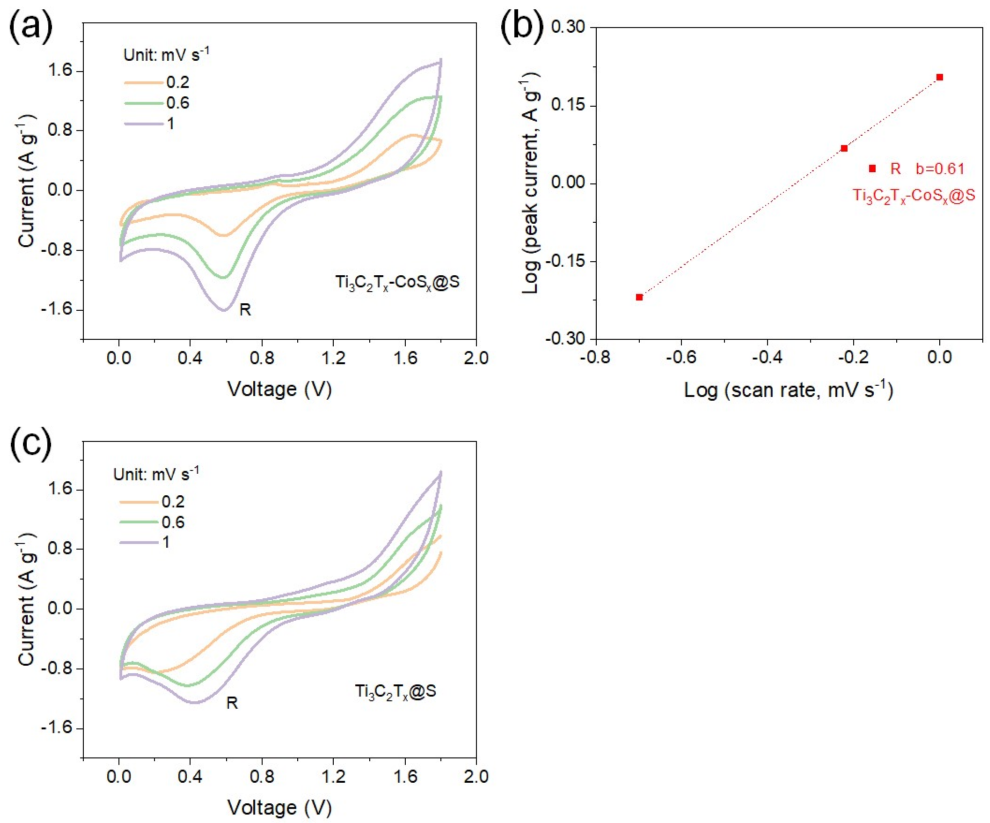

Figure S11. (a) CV curves of $Ti_3C_2T_x$-CoS_x@S cathode at sweep rates of 0.2~1 mV s^{-1}. (b) Logarithmic curve of peak current versus sweep rate from (a). (c) CV curves of $Ti_3C_2T_x$@S cathode at sweep rates of 0.2~1 mV s^{-1}.

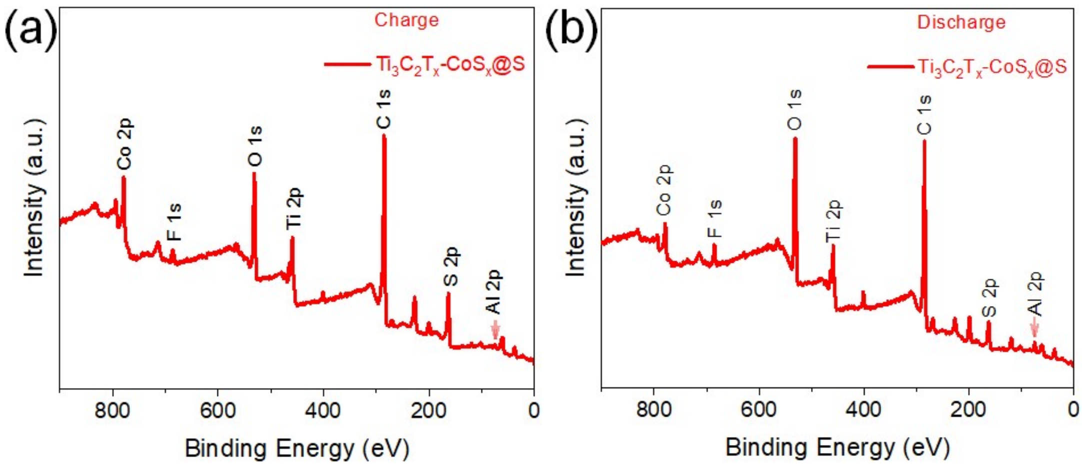

Figure S12. XPS full-spectra of $Ti_3C_2T_x$-CoS_x@S cathodes at charged-1.8 V (a) and discharged-0.01 V (b) states.

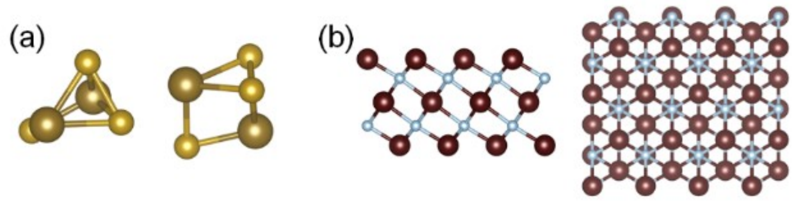

Figure S13. (a) The molecular structures of Al_2S_3. (b) Side (left) and top (right) views of the optimized structure of $Ti_3C_2T_x$ monolayer.

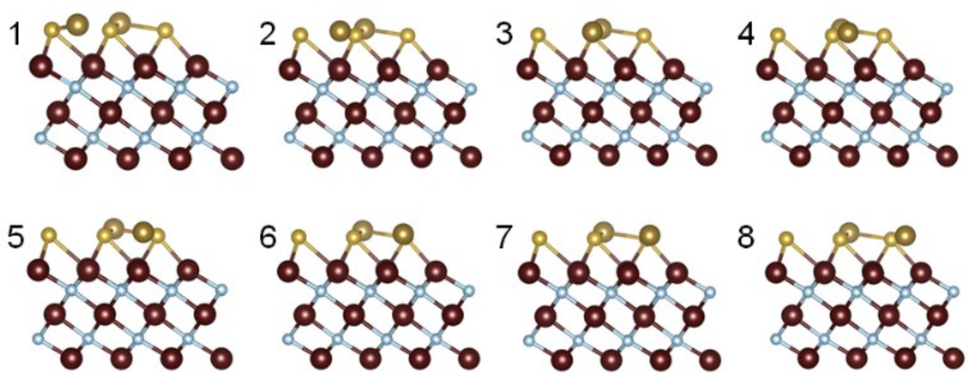

Figure S14. Side views of the stable adsorption and dissociation configurations of Al_2S_3

on $Ti_3C_2T_x$ monolayer.

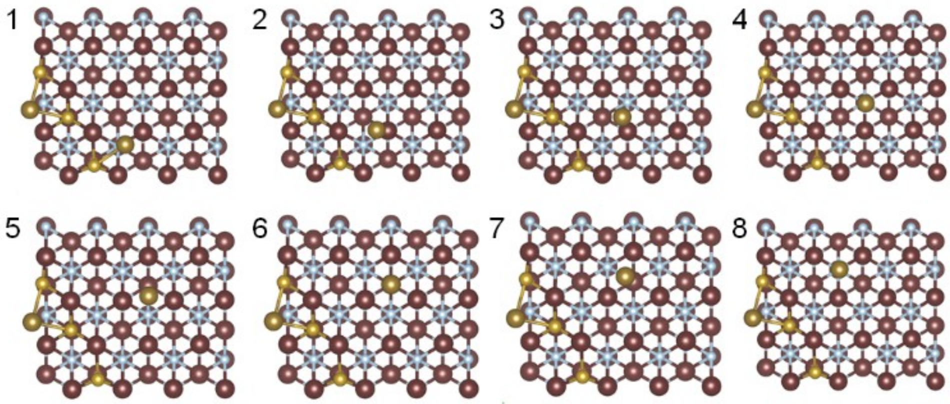

Figure S15. Top views of the stable adsorption and dissociation configurations of Al_2S_3 on $Ti_3C_2T_x$ monolayer.

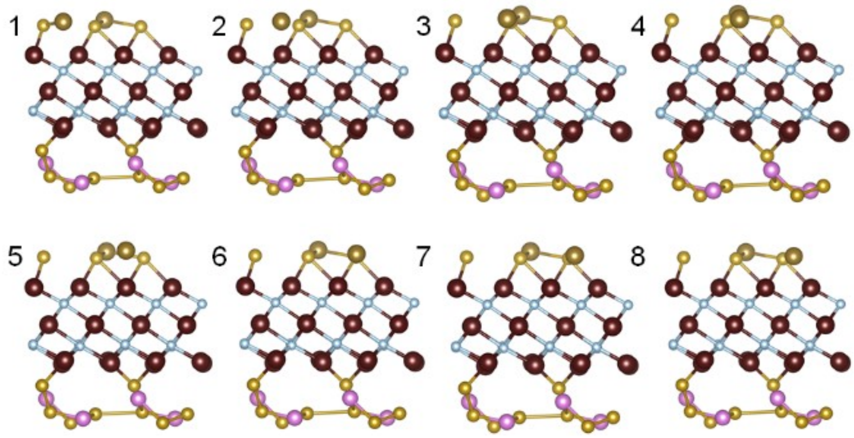

Figure S16. Side views of the stable adsorption and dissociation configurations of Al_2S_3 on $Ti_3C_2T_x$−CoS_2 heterostructure surface.

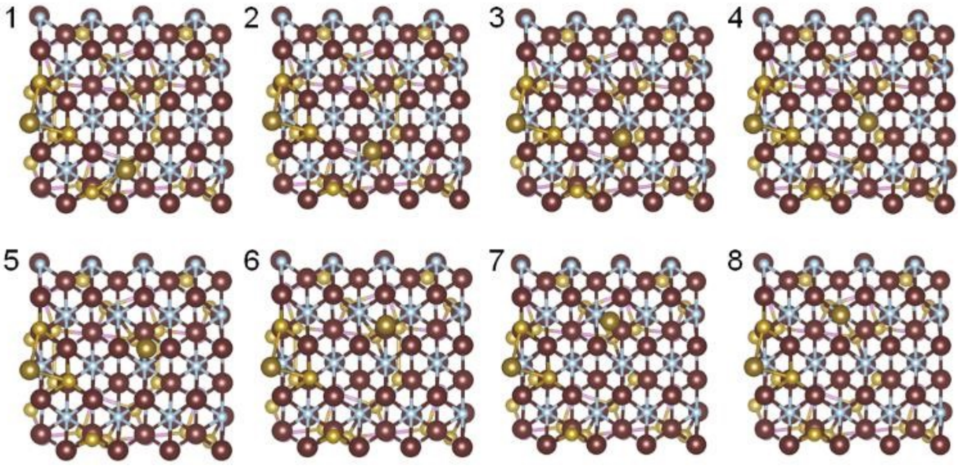

Figure S17. Top views of the stable adsorption and dissociation configurations of Al_2S_3 on $Ti_3C_2T_x$−CoS_2 heterostructure surface.

Table S1. Comparison of the electrochemical performance of $Ti_3C_2T_x$-CoS_x@S cathode in this work with other cathode materials reported for AIBs.

Cathodes	Initial capacity (mAh g^{-1})	Final capacity (mAh g^{-1})	Rate (mA g^{-1})	CE (%)	Ref.
ZnSe/$SnSe_2$	386	124 (150th)	100	98	[2]
Co_3Se_4/ZnSe@C	207	116 (500th)	200	95	[3]
$CoSe_2$@TiO_2/Ti_3C_2	100	102 (500th)	1600	80	[4]
Co_9S_8 NP@NPC@MXene	160	111 (1000th)	1000	98	[5]
MXene@BDTO	229	134 (500th)	500	98	[6]
TBAOH-FL-V_2CT_x	190	80 (100th)	200	95	[7]
Ti_3C_2@CTAB-Se	250	132 (400th)	200	95	[8]
Cu/MoO_2@C@S	967	254 (100th)	500	98	[9]
$Ti_3C_2T_x$-CoS_x@S	358 308	215 (1000th) 190 (1500th)	1000 1500	100	This work

References

1. X. Zheng, Z. Wang, J. Li and L. Wei, Binder-free S@$Ti_3C_2T_x$ sandwich structure film as a high-capacity cathode for a stable aluminum-sulfur battery, *Sci. China Mater.*, 2022, **65**, 1463-1475.

2. J. Li, W. Luo, Z. Zhang, F. Li, Z. Chao and J. Fan, ZnSe/$SnSe_2$ hollow microcubes as cathode for high performance aluminum ion batteries, *J. Colloid Interface Sci.*, 2023, **639**, 124-132.

3. T. Liu, G. Lv, M. Liu, C. Zhao, L. Liao, H. Liu, J. Shi, J. Zhang and J. Guo, Synergistic Transition-Metal Selenide Heterostructure as a High-Performance Cathode for Rechargeable Aluminum Batteries, *ACS Appl. Mater. Interfaces*, 2023, **15**, 11906-11913.

4. Z. Yuan, Q. Lin, Y. Li, W. Han and L. Wang, Effects of Multiple Ion Reactions Based on a $CoSe_2$/MXene Cathode in Aluminum-Ion Batteries, *Adv. Mater.*, 2023, **35**, 2211527.

5. L. Yao, S. Ju and X. Yu, Rational surface engineering of MXene@N-doped hollow carbon dual-confined cobalt sulfides/selenides for advanced aluminum batteries, *J. Mater. Chem. A*, 2021, **9**, 16878-16888.

6. G. Wu, C. Lv, W. Lv, X. Li, W. Zhang and Z. Li, Anthraquinone derivatives supported by Ti_3C_2(MXene) as cathode materials for aluminum-organic batteries, *J. Energy Chem.*, 2022, **74**, 174-183.

7. A. VahidMohammadi, A. Hadjikhani, S. Shahbazmohamadi and M. Beidaghi, Two-Dimensional Vanadium Carbide (MXene) as a High-Capacity Cathode

Material for Rechargeable Aluminum Batteries, *ACS Nano*, 2017, **11**, 11135-11144.

8. Z. Li, X. Wang, W. Zhang and S. Yang, Two-dimensional Ti_3C_2@CTAB-Se (MXene) composite cathode material for high-performance rechargeable aluminum batteries, *Chem. Eng. J.*, 2020, **398**, 125679.

9. Q. Zhou, X. Jiang, X. Zhang, D. Wang, G. Yang, H. Zhou, Y. Wu, F. Guo, M. Chen, G. Diao and L. Ni, Polyoxomolybdate-Based Metal-Organic Framework-Derived Cu-Embedded Molybdenum Dioxide Hybrid Nanoparticles as Highly Efficient Electrocatalysts for Al-S Batteries, *ChemSusChem*, 2024, **n/a**, e202400424.